Materials Science and Engineering C 50 (2015) 266–273

Contents lists available at ScienceDirect

Materials Science and Engineering C

journal homepage: www.elsevier.com/locate/msec

Investigation on the physical–mechanical properties of dental resin composites reinforced with novel bimodal silica nanostructures

Ruili Wang [a], Maolin Zhang [b], Fengwei Liu [a], Shuang Bao [a], Tiantian Wu [c], Xiaoze Jiang [a], Qinghong Zhang [a], Meifang Zhu [a,*]

[a] State Key Laboratory for Modification of Chemical Fibers and Polymer Materials, College of Material Science and Engineering, Donghua University, Shanghai 201620, PR China
[b] Department of Oral and Maxillofacial Surgery, Shanghai 9th People's Hospital, Shanghai Jiao Tong University School of Medicine, Shanghai Key Laboratory of Stomatology, Shanghai 200011, PR China
[c] Department of General Dentistry, Shanghai 9th People's Hospital, Shanghai Jiao Tong University School of Medicine, Shanghai Key Laboratory of Stomatology, Shanghai 200011, PR China

ARTICLE INFO

Article history:
Received 26 May 2014
Received in revised form 5 January 2015
Accepted 30 January 2015
Available online 2 February 2015

Keywords:
Bimodal silica nanostructures
Filler compositions
Resin composites
Polymerization shrinkage
Mechanical properties
Cytotoxicity assay

ABSTRACT

The aim of this study was to investigate the influence of bimodal silica nanostructures comprising of SiO_2 nanoparticles (SiO_2 NPs, ~70 nm) and SiO_2 nanoclusters (SiO_2 NCs, 0.07–2.70 μm) on physical–mechanical properties of resin-based composites (RBCs). SiO_2 NPs and SiO_2 NCs were prepared with the Stöber method and the coupling reaction, respectively, then silanized and employed as fillers to construct RBCs using a mixture of bisphenol A glycerolate dimethacrylate (Bis-GMA) and tri(ethylene glycol) dimethacrylate (TEGDMA) as the organic matrix. Results showed that the properties of RBCs were influenced by the filler ratios of bimodal silica nanostructures, and the appropriate amount of SiO_2 NPs could effectively increase the activating light efficiency and filler packing density of RBCs. Among all experimental RBCs, RBC 50–20 (SiO_2 NPs:SiO_2 NCs = 50:20, wt/wt) presented the highest degree of conversion (71.6 ± 1.1%), the lowest polymerization shrinkage (2.6 ± 0.1%), and the enhanced flexural strength (104.8 ± 4.4 MPa), flexural modulus (6.2 ± 0.3 GPa), and compressive strength (205.8 ± 14.3 MPa), which were improved by 44%, 19%, 28%, 48%, and 42% in comparison with those of RBC 0–60 (SiO_2 NPs:SiO_2 NCs = 0:60, wt/wt), respectively. Besides, in vitro cytotoxicity evaluation of RBC 50–20 indicated its acceptable cytotoxicity. Although the best performance was achieved by commercial Z350 XT, the introduction of bimodal silica nanostructures might provide the enhanced physical–mechanical properties of RBCs, compared with those of RBC 0–60 reinforced with unimodal SiO_2 NCs.

1. Introduction

Clinical use of light-cured dental restorative composites has increased rapidly due to their distinguished esthetics and biocompatibility, compared with metallic dental amalgams [1]. However, the main reason for failure is still secondary caries followed by fracture of restoration [2,3].

Resin-based composites (RBCs) generally consisted of a polymeric matrix admixed with silanized inorganic fillers and photo-initiators, and could be cured to form the polymer network structure under the light irradiation. The development of RBCs has resulted in the optimization of filler types, compositions and loading, leading to an enhancement in their physical–mechanical properties [4–7]. Satterthwaitea et al. [6,7] found out that shrinkage values were lower for RBCs containing different sizes of spherical fillers with appropriate weight ratios compared to those with irregular fillers. Wang et al. [8] introduced the novel porous diatomite and nano-sized silica particles as co-fillers to increase the mechanical performance of RBCs by regulating their filler compositions. These works are related to the development of hybrid RBCs, which have been launched into the dental market and widely used in clinical application, owing to their intermediate esthetics and excellent mechanical performance compared with macro-filler and micro-filler based composites [9].

A recent response to the challenge of combining excellent esthetics and mechanical performance is the application of nanotechnology, and thus "nanoclusters (NCs)" described as a combination of individually dispersed nano-sized particles and their agglomerations have been introduced as inorganic fillers to meet all requirements of both posterior and anterior restorations to the most degree [10]. The latest commercial product is Z350 XT (3M ESPE, St. Paul, MN, USA) containing silica and zirconia nanoparticles (NPs), which are partially calcined to prepare micron-sized cluster fillers using the "bottom to top" method and then silanized prior to mixing with polymer matrix. These NCs provide a distinct reinforcing mechanism and the improved resistance to crack propagation and water corrosion, compared with micro-filler or hybrid based composites, resulting in the significant improvement in the

* Corresponding author.
E-mail address: zhumf@dhu.edu.cn (M. Zhu).

http://dx.doi.org/10.1016/j.msec.2015.01.090
0928-4931/

Table 1
Compositions of the commercial resin composites (RBCs).

Resin composite	Matrix type	Particle type	Manufacturer
Esthet-X (Shade A3)	• Bis-GMA • Bis-EMA • TEGDMA	• Silicate glass particles (<1 μm) • Nanosilica (0.04 μm) • Filler loading: 77 wt.%	Dentsply, York, PA, USA
Z350 XT (Shade A3)	• Bis-GMA • UDMA • TEGDMA • Bis-EMA (6) • PEGDMA	• Non-agglomerated/non-aggregated silica filler (20 nm) • Non-agglomerated/non-aggregated zirconia filler (4–11 nm) • Aggregated zirconia/silica cluster filler (0.6–10 μm) • Filler loading: 78.5 wt.%	3M ESPE, St. Paul, MN, USA

Bis-GMA is bisphenol A glycerolate dimethacrylate.
Bis-EMA is ethoxylated bisphenol A glycol dimethacrylate.
TEGDMA is tri(ethylene glycol) dimethacrylate.
UDMA is urethane dimethacrylate.
Bis-EMA (6) is hexaethoxylated bisphenol A glycol dimethacrylate.
PEGDMA is polyethylene glycol dimethacrylate.

strength and the longevity of the restoration [11,12]. However, the new preparative ways of cluster fillers suitable for resin restorative applications and the relevant reinforcing mechanism still need to be explored clearly.

In our previous work, RBCs with bimodal silica nanostructures including SiO_2 NPs and SiO_2 NCs as fillers at the optimum weight ratio have been developed and confirmed to possess excellent wear resistance, due to the reduced interparticle spacing and the increased filler packing, leading to the lower wear volume and the smoother worn surface with respect to that of the microhybrid Esthet-X (Dentsply, York, PA, USA), which was also comparable with that of Z350 XT [13]. Therefore, as a continuation of this work, the relevant physical–mechanical properties will be further estimated so as to investigate the effect of the bimodal silica nanostructures on degree of conversion, polymerization shrinkage, mechanical performance, as well as the cytotoxicity of RBCs, compared with those of Esthet-X and Z350 XT.

2. Materials and methods

2.1. Materials

Anhydrous ethanol, tetraethoxysilane (TEOS), ammonia solution (25–28 wt.%), cyclohexane, n-propylamine, and 3-methacryloxypropyl trimethoxysilane (γ-MPS) were received from Sinopharm Chemical Reagent Co., Ltd (SCRC, Shanghai, China). 3-Aminopropyl triethoxysilane (APTES), 3-glycidoxypropyl trimethoxysilane (GPS), bisphenol A glycerolate dimethacrylate (Bis-GMA), tri(ethylene glycol) dimethacrylate (TEGDMA), camphorquinone (CQ) and ethyl 4-dimethylamino benzoate (4-EDMAB) were purchased from Sigma-Aldrich Chemical Co. (Milwaukee, USA). Human dental pulp cells (HDPCs) were obtained from Shanghai Ninth People's Hospital Affiliated Shanghai Jiaotong University School of Medicine (Shanghai, China). Dulbecco's modified eagle's medium (DMEM; Gibco, Grand Island, NY, USA), fetal bovine serum (FBS; Hyclone, Logan, UT, USA), penicillin and streptomycin (Shanghai Sanda Jinyi Tech Info Co., Ltd., Shanghai, China), 3-(4,5-dimethylthiazol-2-yl)-2,5-diphenyltetrazolium bromide (MTT; Sigma-Aldrich, Milwaukee, USA), dimethyl sulfoxide and glutaraldehyde (Simopharm Chemical Reagent Co., Shanghai, China) were acquired and used as received. Furthermore, commercial microhybrid Esthet-X (Dentsply, York, PA, USA) and nanocomposite Z350 XT (3M ESPE, St. Paul, MN, USA) were introduced as controls in this work, which were specified in Table 1, based on their technical profile.

2.2. Methods

2.2.1. Silanization of inorganic fillers

Inorganic fillers consisted of SiO_2 NPs (~70 nm) and SiO_2 NCs (0.07–2.70 μm), which were prepared using the Stöber method and the coupling reaction between epoxy and amino functionalized SiO_2 NPs, respectively, according to our previous work [13]. Subsequently, these

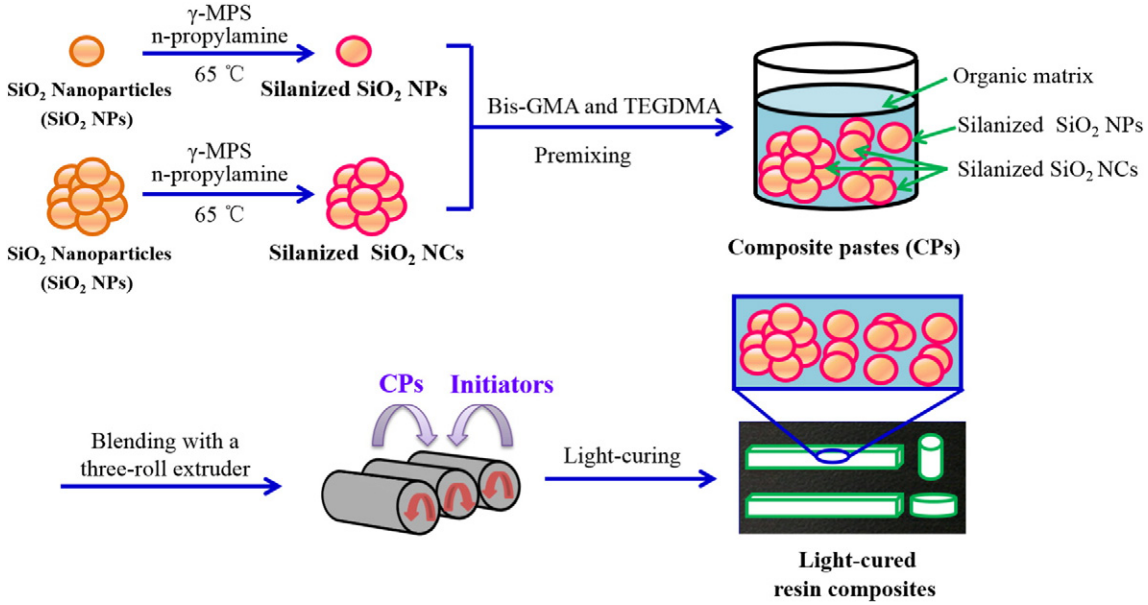

Fig. 1. Representative scheme of the fabrication of light-cured resin composites with silanized SiO_2 NPs and SiO_2 NCs.

inorganic particles were silanized with γ-MPS to introduce vinyl functional groups on their surface so as to polymerize with methacrylate-based resin matrix during the light-curing process.

2.2.2. Preparation of experimental RBCs

Experimental RBCs were fabricated following our reported procedure [13], and the representative scheme was presented in Fig. 1. Silanized filler particles were premixed with resin matrix (Bis-GMA/TEGDMA = 70/30, wt/wt), and then thoroughly blended into a three-roll extruder (EXAKT 80E, Exakt Apparatebau GmbH & Co., Norderstedt, Germany) with photo-initiators (CQ/4-EDMAB = 0.2/0.8, wt/wt). The weight fractions of inorganic fillers were 60 wt.% and 70 wt.%, and mass ratios of SiO_2 NPs to SiO_2 NCs were fixed at 0:60, 25:45, 30:40, 35:35, 40:30, 50:20, 53:17, 60:0, and 70:0, respectively.

The obtained uncured RBC pastes were placed into the silicon rubber molds, covering the surface with a glass slide, and photo-polymerized with a LED curing unit (SLC-VIII B, 430–490 nm, 1000 mW/cm^2, Hangzhou Sifang Medical Apparatus Co., Ltd., Zhejiang, China) for 60 s on each side. The distance between the light tip and the sample surface was kept at 3–5 mm. The prepared RBCs were then stored in the dark for 2–3 days at room temperature, and polished with progressively silicon carbide abrasive papers before testing.

Among all materials, RBC 0–60 (SiO_2 NPs:SiO_2 NCs = 0:60, wt/wt) was filled with the maximum content of silanized SiO_2 NCs, while RBC 25–45 (SiO_2 NPs:SiO_2 NCs = 25:45, wt/wt) and RBC 53–17 (SiO_2 NPs:SiO_2 NCs = 53:17, wt/wt) represented their limit compositions, respectively, which suggested the corresponding RBC pastes could turn into discontinuous fragments if more fillers were introduced. Besides, RBC 0–60 and RBC 0–70 were filled with 60 wt.% and 70 wt.% silanized SiO_2 NPs, respectively [13].

2.3. Characterization

2.3.1. Degree of conversion

Degree of conversion (DC) of RBCs was analyzed on a FTIR spectrometer (Nicolet 8700, Bruker Optik GmbH, Ettlingen, Germany), equipped with an attenuated total reflectance crystal (ATR), operating with 32 scans at a resolution of 4 cm^{-1}. FT-IR spectra were recorded for each RBC before and after curing. Then, DC of each RBC was determined from the ratio of absorbance intensities of aliphatic C═C bond (1638 cm^{-1}) against internal standard of aromatic C═C bond (1608 cm^{-1}) [14]. Three trials were conducted for each material. The DC (%) was then calculated from formula (1):

$$DC(\%) = (1 - R_{cured}/R_{uncured}) \times 100 \quad (1)$$

where R = band height at 1638 cm^{-1}/band height at 1608 cm^{-1}.

2.3.2. Polymerization shrinkage

Polymerization shrinkage was calculated from the densities measured according to the Archimedes' principle [15]. Each specimen of uncured and cured RBCs was carefully stuck on a light fiber and fixed on the steelyard hook of the balance, so the weight of each sample in air and in deionized water was measured with an electronic balance accurate to ±0.001 g (JA5003, Changzhou Keyuan Electronic Instrument Co., Ltd., China, n = 5) [16], and thus the density of each specimen before and after curing was calculated using the following relation (2) [17].

$$\rho = \left(\frac{m_a}{m_a - m_w}\right) \times (\rho_w - \rho_a) + \rho_a \quad (2)$$

Where ρ = the density of sample (g/cm^3), m_a = the mass of the sample in air (g), m_w = the mass of sample in deionized water (g), ρ_w = the density of deionized water at the exactly measured temperature (g/cm^3), and ρ_a = the density of air (0.0012 g/cm^3).

Finally, the polymerization shrinkage of each specimen was determined by the following Eq. (3) [17]:

$$\text{Polymerization shrinkage } (\%) = \left(\frac{\rho_{cured} - \rho_{uncured}}{\rho_{cured}}\right) \times 100 \quad (3)$$

where $\rho_{uncured}$ = the density of the uncured specimen (g/cm^3), ρ_{cured} = the density of the cured specimen (g/cm^3).

2.3.3. Mechanical properties

(1) Flexural strength and flexural modulus.
Six rectangular-shaped specimens (25 mm × 2 mm × 2 mm) were prepared from each RBC pastes and irradiated for 90 s from each side. According to ANSI/ADA specification NO. 27-2009 (ISO-4049), flexural strength (FS) and flexural modulus (FM) of the cured RBCs were measured by a three-point bending test using a universal testing machine (WDW-300, Changchun Kexin Equipment Co., Ltd., Changchun, China), with 20 mm span and 0.75 mm/min cross-head speed.

(2) Compressive strength.
Compressive strength (CS) of RBCs was also evaluated by a universal testing machine with cylindrical specimens (Φ 4 mm × 6 mm) and cross-head speed of 0.75 mm/min. Six samples were loaded to failure in compression.

2.3.4. Cross-section morphologies

A field scanning electron microscope (S-4800 Hitachi, Tokyo, Japan) was used to investigate the fracture surfaces of RBCs after the three-point bending tests, operating at 5 kV.

2.3.5. Cell viability assays

(1) Isolation and culture of HDPCs.
All procedures were approved by the Ethics Committee of Shanghai Ninth People's Hospital Affiliated to Shanghai Jiao Tong University School of Medicine. Informed consent was obtained from each patient. Dental pulp tissue was isolated from premolars or third molars as previously described [18]. The isolated pulp tissue was minced into 1–2 mm^3 pieces, and then plated in a petri dish and cultured in DMEM containing 20% FBS, 0.5% penicillin, and 0.5% streptomycin at 37 °C in 5% CO_2. The culture

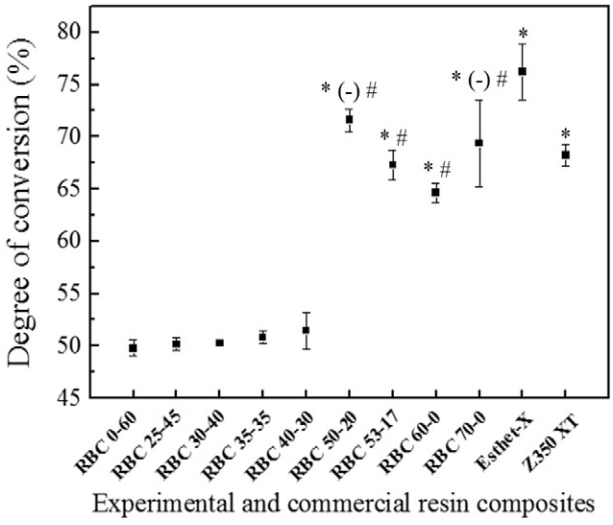

Fig. 2. Degree of conversion of experimental resin composites reinforced with silanized SiO_2 NPs and SiO_2 NCs of different mass ratios, as well as commercial Esthet-X and Z350 XT. *p < 0.01, compared with RBC 0–60; (−) p > 0.01, compared with Esthet-X; #p > 0.01, compared with Z350 XT.

medium was changed every three days. HDPCs isolated from dental pulp tissue at passages 3 were used for this study.

(2) MTT assay.
A total of 10^4 HDPCs per well were plated in 48-well tissue culture plates (TCPs), and their viability on selected RBCs (RBC 0–60, RBC 50–20, RBC 70–0, Esthet-X and Z350 XT) with the size of Φ 10 mm × 1 mm was evaluated using MTT assay [19]. At different time points (1, 3, and 5 days) after initiation of culture, 50 μL MTT (0.5 mg/mL) was added into each well for additional 4 h incubation. Subsequently, the medium was subsequently removed, and 300 μL DMSO was added to dissolve the formazan crystals. Then, the optical density was measured at a wavelength of 490 nm using a microplate reader (Elx 800, Bio-Tek, Burlington, VT, USA). Mean and standard deviation for the triplicate wells for each sample were reported.
To further examine the cytotoxicity, the morphology of HDPCs grown onto these five selected RBCs was characterized with FE–SEM. Before analysis, cells grown onto different composite samples were fixed with 2% glutaraldehyde for 2 h at 4 °C, dehydrated with a series of gradient ethanol solutions (50%, 70%, 80%, 90%, 95%, and 100% vol.%) for 10 min each, and air-dried. Then, the samples were gold sputter-coated and observed by FE–SEM (S-4800 Hitachi, Tokyo, Japan) with an operating voltage of 10 kV.

2.3.6. Statistical analysis

One-way analysis of variance (ANOVA) was performed to determine the statistical significance of all experimental data, using SPSS 13.0 software. In all evaluations, $p < 0.01$ was considered statistically significant.

3. Results

3.1. Degree of conversion

DC values of all RBCs are presented in Fig. 2. Compared with the lowest DC of RBC 0–60 (49.8 ± 0.8%), RBC 60–0 and RBC 70–0 presented the significantly higher value of 64.6 ± 1.0% and 69.4 ± 4.1% ($p < 0.01$), respectively, which was still lower than that of RBC 50–20 (71.6 ± 1.1%, $p < 0.01$) and RBC 53–17 (67.3 ± 1.4%, $p < 0.01$), with the increasing amount of SiO_2 NPs in bimodal silica nanostructures. Moreover, the conversion value of RBC 50–20 and RBC 70–0 did not show statistical significant difference ($p > 0.01$), in comparison with Esthet-X (76.2 ± 2.6%) and Z350 XT (68.3 ± 1.0%), respectively.

3.2. Polymerization shrinkage

Polymerization shrinkage for RBCs with different mass ratios of SiO_2 NPs and SiO_2 NCs is depicted in Fig. 3. It could be observed that all shrinkage values of the following materials RBC 0–60 (3.2 ± 0.1%), RBC 60–0 (3.4 ± 0.1%), RBC 70–0 (3.1 ± 0.1%), and Esthet-X (3.3 ± 0.1%) were above 3.0%. Compared with RBC 0–60, the shrinkage was decreased from 2.9 ± 0.1% for RBC 25–45 to the lowest 2.6 ± 0.1% for RBC 50–20 ($p < 0.01$), and then increased slightly to 2.7 ± 0.2% for RBC 53–17 ($p < 0.01$), with the increasing content of SiO_2 NPs in RBCs blended with bimodal silica nanostructures, which were also significantly lower than that of Esthet-X ($p < 0.01$). Although the lowest shrinkage was achieved by Z350 XT (2.5 ± 0.1%), both RBC 50–20 and RBC 53–17 showed no difference compared with this control group ($p > 0.01$).

3.3. Mechanical properties

Mechanical properties of all RBCs are displayed in Fig. 4. For materials reinforced with unimodal inorganic fillers, RBC 0–60 exhibited the lowest FS, FM, and CS of 82.0 ± 6.1 MPa, 4.0 ± 0.2 GPa, and 144.6 ± 7.6 MPa, respectively, which were similar with those of RBC 60–0, but significantly lower than those of RBC 70–0 (94.3 ± 3.1 MPa, 5.8 ± 0.8 GPa, and 160.3 ± 6.9 MPa; $p < 0.01$) with higher filler loading.

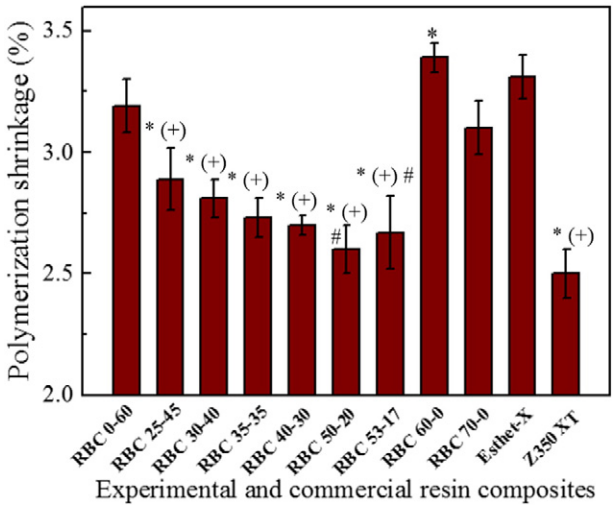

Fig. 3. Polymerization shrinkage of experimental resin composites blended with silanized SiO_2 NPs and SiO_2 NCs of different mass ratios, as well as commercial Esthet-X and Z350 XT. *$p < 0.01$, compared with RBC 0–60; (+) $p < 0.01$, compared with Esthet-X; #$p > 0.01$, compared with Z350 XT.

Fixing the filler content to 70 wt.% of RBCs reinforced with bimodal silica nanostructures, their mechanical properties presented a gradual increase to the maximum for RBC 50–20 (104.8 ± 4.4 MPa, 6.2 ± 0.3 GPa, and 205.8 ± 14.3 MPa), and then a slight decrease for RBC 53–17 with the increasing supplement of SiO_2 NPs, which were significantly lower than those of Z350 XT (FS: 120.8 ± 4.9 MPa, FM: 8.1 ± 0.5 GPa, and CS: 253.9 ± 5.0 MPa), respectively ($p < 0.01$). While, compared with another control group Esthet-X (110.6 ± 3.3 MPa, 5.0 ± 0.2 GPa, and 232.0 ± 16.6 MPa), the optimum RBC 50–20 showed a significantly higher FM ($p < 0.01$) and no significant difference in FS and CS ($p > 0.01$).

3.4. Cross-sectional morphologies

Fracture morphologies of representative RBCs after the three-bending tests are presented in Fig. 5. It clearly showed that inorganic particles of all RBCs were well adhered to the resin matrix without exposed fillers examined.

3.5. In vitro cytotoxicity analysis

Fig. 6 shows the cell viability of TCPs and selected RBCs under the different culture time. Compared with TCPs, it could be clearly observed that the viability of HDPCs on all RBCs showed significant difference ($p < 0.01$), except that of Esthet-X after 1 day culture ($p > 0.01$) and RBC 50–20 after 3 days of culture ($p > 0.01$), respectively. The viability of HDPCs cultured onto RBC 50–20 was much higher than that onto RBC 0–60 after 1 day and 3 days of culture ($p < 0.01$), and showed no difference at the time point of 5 days ($p > 0.01$). For the optimum RBC 50–20, more attention should be focused on its cell viability compared with commercial products. As can be seen from Fig. 6 that the viability of RBC 50–20 was significantly lower than that of Esthet-X after 1 day culture first ($p < 0.01$), which showed no significant difference on culture days of 3 and 5 ($p > 0.01$). While, for the other control group, statistical significant difference was assessed for RBC 50–20 and Z350 XT after each culture period ($p < 0.01$). Furthermore, FE–SEM micrographs in Fig. 7 present that all RBCs were able to allow HDPCs to be attached at the different culture time, and the detailed cell morphology could be observed from the insets showing the magnified region, as the arrows indicated. RBC 50–20 had the similar cell attachment viability to the

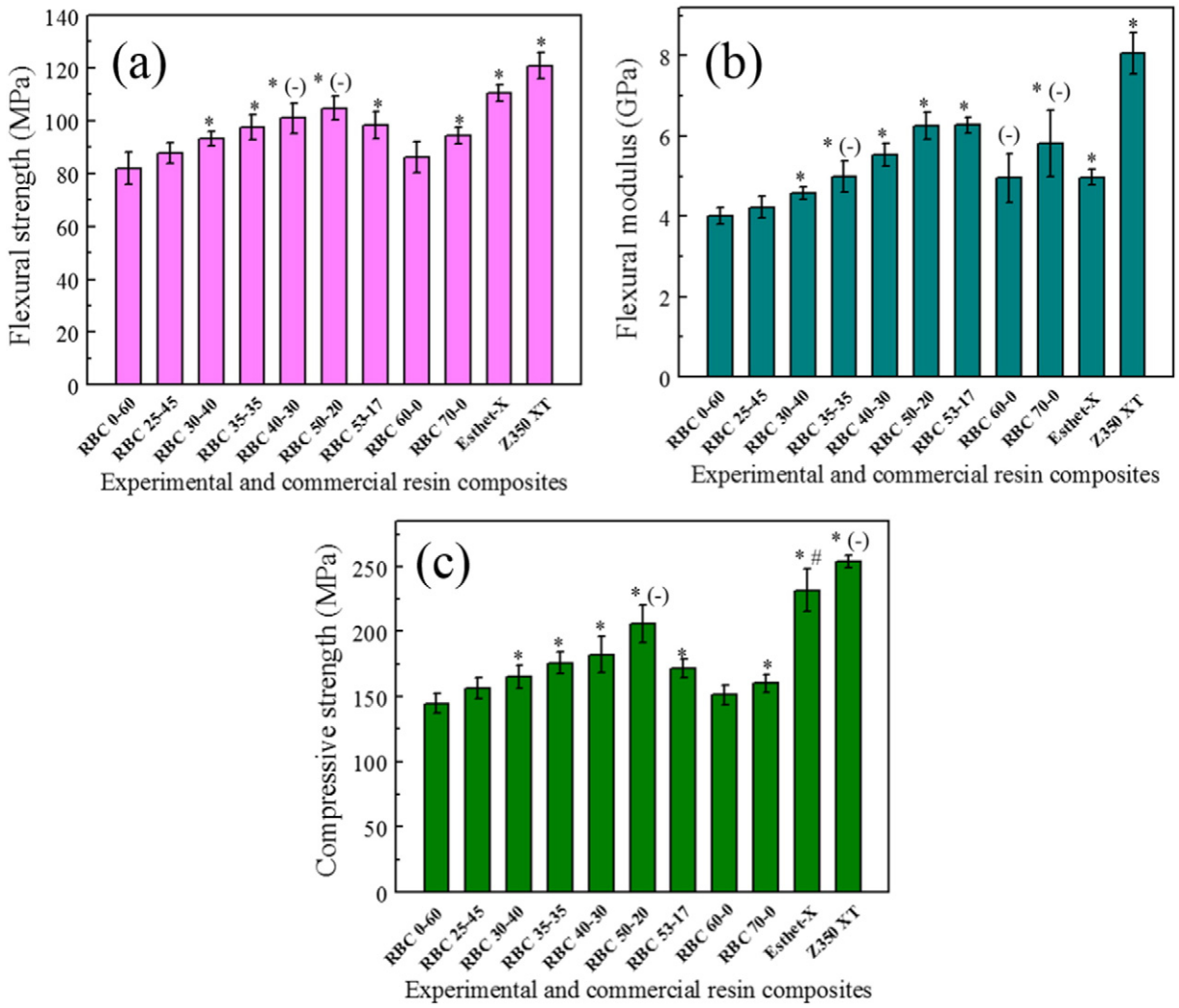

Fig. 4. Mechanical properties of experimental resin composites filled with silanized SiO_2 NPs and SiO_2 NCs of different mass ratios, as well as commercial Esthet-X and Z350 XT: flexural strength (a), flexural modulus (b), and compressive strength (c). *$p < 0.01$, compared with RBC 0–60; (−) $p > 0.01$, compared with Esthet-X; #$p > 0.01$, compared with Z350 XT.

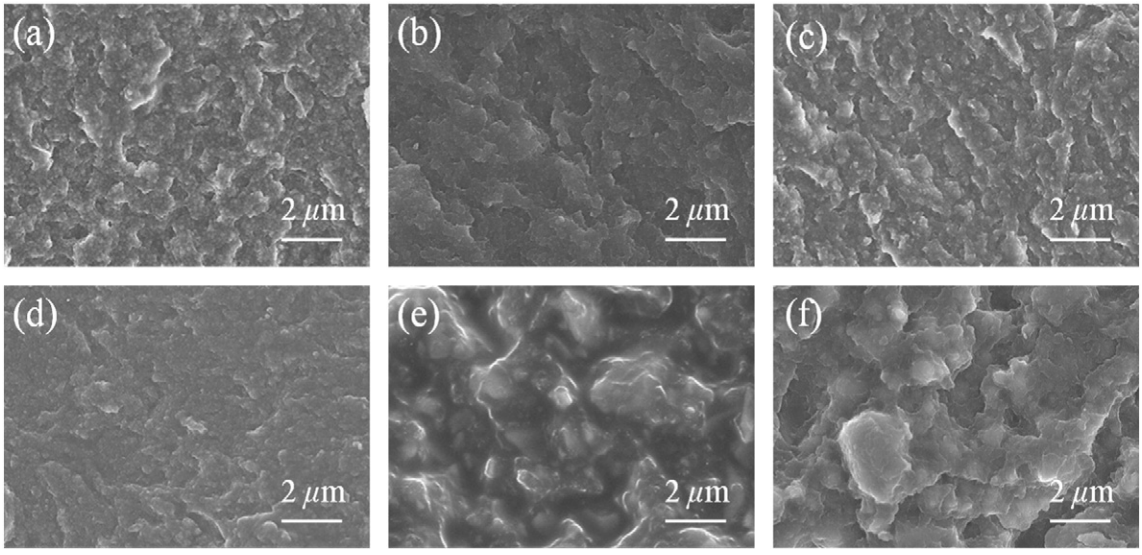

Fig. 5. FE–SEM images of the fracture surfaces of representative resin composites after the three-point bending tests: RBC 0–60 (a), RBC 50–20 (b), RBC 60–0 (c), RBC 70–0 (d), Esthet-X (e), and Z350 XT (f), respectively.

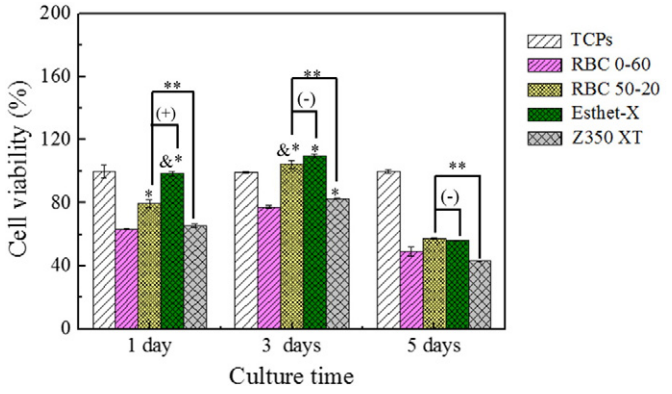

Fig. 6. MTT assay of HDPCs viability cultured onto TCPs, RBC 0–60, RBC 50–20, Esthet-X, and Z350 XT, respectively. &p > 0.01, compared with TCPs; *p < 0.01, compared with RBC 0–60; (+) p < 0.01, compared with Esthet-X; (−) p > 0.01, compared with Esthet-X; **p < 0.01, compared with Z350 XT.

control of Esthet-X after 3, and 5 days of culture, respectively. While, less HDPCs were penetrated onto RBC 0–60 and Z350 XT. The cell morphology observation results corroborated the MTT assay data.

4. Discussion

All experimental RBCs were incorporated with different filler compositions, and it has been proved that the combination of relatively small and varied size fillers could provide a more dense packing, leading to the increased filler fraction and the fracture strength of composite materials [13,20]. Therefore, in this present work, the filler loading of RBCs could be increased to 70 wt.% with the introduction of SiO_2 NPs, compared with that of RBC 0–60 reinforced with SiO_2 NCs only. Based on the improved wear resistance of RBCs reinforced with bimodal silica nanostructures [13], their effect on the other properties, such as DC, polymerization shrinkage, mechanical performance, and cytotoxicity assay in vitro were investigated. It should be noted that even the size of SiO_2 NCs reached to several micrometers, their constituent was still based on SiO_2 NPs, which could help us to explore the inherent mechanism of RBCs reinforced with bimodal silica nanostructures.

4.1. Degree of conversion

DC values of all RBCs are presented in Fig. 2. Among all RBCs studied, flowable Esthet-X was examined to exhibit the highest conversion of 76.2 ± 2.6%, which might be explained by the high reactivity and conversion produced by a greater proportion of diluents, such as TEGDMA and Bis-EMA [21].

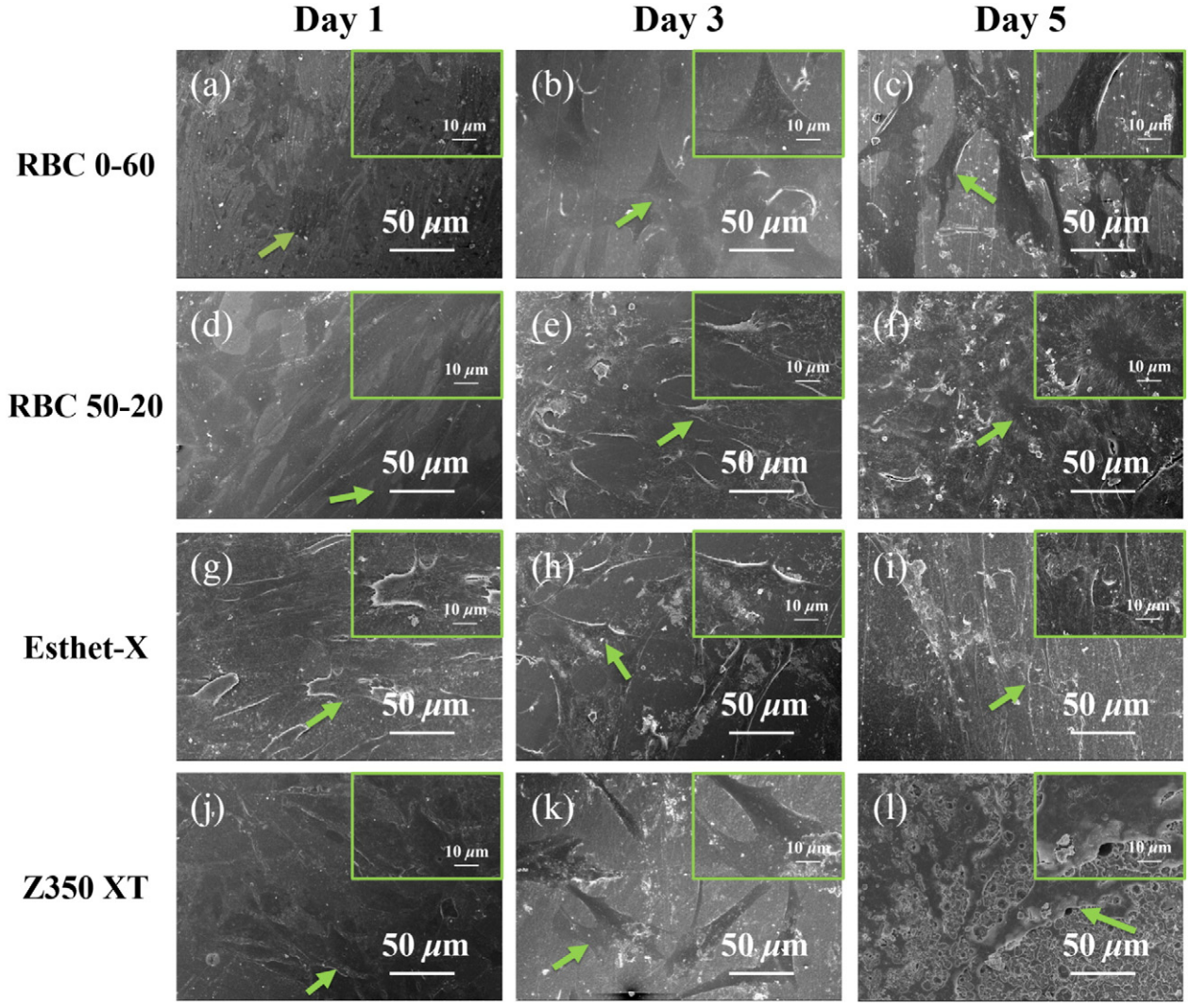

Fig. 7. FE–SEM images of HDPCs grown onto RBC 0–60, RBC 50–20, Esthet-X, and Z350 XT after 1, 3, and 5 days of culturing, respectively. The insets show the magnified surface details as the arrows indicated.

On the other hand, DC might also be affected by inorganic fillers. For RBCs reinforced with unimodal fillers, due to the higher light scattering of smaller filler particles, the DC of RBC 60–0 was higher than that of RBC 0–60 [22], which was slightly increased for RBC 70–0, due to the increased activating light efficiency from multiple light scattering by filler particles at higher filler loading [23]. Furthermore, for RBCs reinforced with bimodal silica nanostructures at 70 wt.% filler loading, different filler compositions should be attributed for their DC trend. As can be seen from Fig. 2, DC values were increased slightly first, and then reached to a maximum for RBC 50–20, which suggested that higher light scattering was obtained with the increasing amount of smaller SiO_2 NPs instead of SiO_2 NCs, and hence higher conversion was achieved [1,22,23]. Additionally, it could be speculated that the average filler particle size of RBC 50–20 was near half the wavelength of the blue light employed, resulting in the highest light transmittance and the maximum DC, according to Ruyter and Øysæd [1,24]. While, the slight decline DC of RBC 53–17 might be due to the decreased average filler size, which deviated slightly from the half wavelength of irradiation light, with the extra SiO_2 NPs added [24]. However, Z350 XT showed the lower DC than that of RBC 50–20, which might be owing to the light attenuation of the wider size distribution of its silica/zirconia cluster fillers (0.6–10 μm) [6,22,25].

4.2. Polymerization shrinkage

Dental RBCs undergo shrinkage during the polymerization process, which is attributed to the conversion of intermolecular Van der Waals distances of the resin-monomers to the covalent bond-lengths, potentially resulting in secondary caries and postoperative pain [26]. Several factors are influential in determining the shrinkage values, such as the monomer structure and content, the filler type and composition, as well as the DC of RBCs [6,27].

Polymerization shrinkage of all RBCs investigated is presented in Fig. 3. Considering the difference in resin matrix, the flowable Esthet-X presented the higher shrinkage ($3.3 \pm 0.1\%$) than that of the rest conventional composites [28], which was in agreement with generally accepted conclusion that the higher conversion resulted in the higher shrinkage of RBCs [21,29]. With respect to inorganic fillers, shrinkage values of RBCs were inversely related to filler loading [25]. Therefore, RBC 60–0 presented the highest shrinkage ($3.4 \pm 0.1\%$), while RBC 70–0 and RBC 0–60 exhibited the similar decreased values, due to the increased filler loading (70 wt.%) and the reduced DC, as discussed above, respectively [25,29].

For composites reinforced with bimodal silica nanostructures, the shrinkage value was reduced abruptly, due to the fact that the number of reactive methacrylate groups in RBCs with high filler levels decreased [30]. Moreover, the shrinkage was decreased with the increasing amount of SiO_2 NPs, which seemed inconsistent with the reported conclusion that higher DC produced higher shrinkage, described by Silikas and Braga [31,32]. However, from the other perspective, the influence of fillers on the shrinkage was also related to their compositions and packing density [6,29]. It could be assumed that with the increasing amount of SiO_2 NPs, the interstices existing in RBCs could be gradually embedded with these small fillers instead of polymeric matrix, potentially resulting in the increased filler packing density, and thus the movement of formed polymer chains might be further hindered during the polymerization process, which finally led to the decrease of the shrinkage to the minimum for RBC 50–20 ($2.6 \pm 0.1\%$). While, RBC 53–17 consisting of extra SiO_2 NPs presented a slight increasing value, which might be due to the relatively less filler packing. However, Z350 XT exhibited the lowest shrinkage ($2.5 \pm 0.1\%$), comparable with that of RBC 50–20 and RBC 53–17, which could also be attributed to its denser packing density, arising from the wider size distribution of silica/zirconia clusters (0.6–10 μm), and their smaller building blocks (20 nm SiO_2 and 4–11 nm ZrO_2), as well as its higher filler content (78.5 wt.%) [30].

4.3. Mechanical properties

Mechanical properties are an essential aspect for evaluating the clinical applications of RBCs, and the obtained results shown in Fig. 4 not only approach those reported for some conventional RBCs reinforced with hybrid fillers (FS = 70–130 MPa, FM = 5–25 GPa, CS = 150–250 MPa) [16,33] but also meet the minimum FS requirement of 80 MPa and 50 MPa for Type I and Type II restorative composites, respectively, according to ISO 4049 [34].

All related data indicated that RBC 0–60 using SiO_2 NCs as unique fillers presented the lowest FS, FM, and CS, which possibly resulted from its lower filler loading and packing. As expected, mechanical properties of composites reinforced with bimodal silica nanostructures were obviously enhanced. That is, with the increasing addition of SiO_2 NPs, the interstices existing in composites might be gradually embedded with SiO_2 NPs rather than resin matrix, accompanying with the increased filler loading and packing, thus resulting in the improved mechanical performance, which was in accordance with the reported work [2,13]. However, less dense packing was achieved by uniform fillers of a narrow size distribution, such as SiO_2 NPs in RBC 60–0 and RBC 70–0, since the interstitial pore volume was maximized [2], and thus leading to their worse mechanical performance. Therefore, bimodal silica nanostructures containing SiO_2 NPs and SiO_2 NCs as co-fillers were introduced.

When the weight ratio of these co-fillers reached an optimum value, the mechanical properties could achieve the maximum for RBC 50–20, which were close to those of Esthet-X, but still significantly lower than those of Z350 XT. However, with the exceeding addition of SiO_2 NPs after the optimum ratio, the amount of "micron-level" SiO_2 NCs was slightly decreased, resulting in the reduced performance for RBC 53–17, due to the worse mechanical characteristic of SiO_2 NPs [8], though the relatively dense filler packing was kept. This trend was mainly in agreement with the filler loading and packing discussed above, and there is no doubt that Z350 XT presented the highest mechanical performance, which could be attributed to its highest filler loading (78.5 wt.%) and the densest filler packing arising from its building block with small size (20 nm SiO_2 and 4–11 nm ZrO_2) [2,8,35].

Preliminary studies focused mainly on the effect of filler type and loading on properties of RBCs [8,25,36], while the filler packing was seldom discussed, however, their objects were usually strived to find the optimum filler compositions, which demonstrated the densest filler packing actually. Therefore, the type, loading, and packing density of inorganic fillers should be three fundamental essentials for designing RBCs with excellent properties. In this present work, the densest filler packing might be obtained for RBC 50–20. Therefore, its fracture surface was further investigated compared with that of Esthet-X and Z350 XT.

4.4. Cross-sectional morphologies

After the three-bending tests, the fracture surfaces of RBCs could be examined by FE-SEM, which reflected the interaction between inorganic fillers and organic matrix. As shown in Fig. 5, inorganic fillers were completely covered without naked or exposed particles observed, which confirmed their excellent interfacial adhesion to the resin matrix, resulting from the chemical bonding between methacrylate groups and hydrophobic interactions in γ-MPS and polymer matrix [37]. Besides, the different sizes of inorganic fillers could be clearly detected in Fig. 5(e) and (f) for Esthet-X and Z350 XT, respectively, which was in agreement with their formulation in Table 1.

4.5. Cytotoxicity assay and cell morphology observation

(1) MTT assay
Among all RBCs examined, the cell viability was speculated in the following order: Esthet-X > RBC 50–20 > Z350 XT > RBC 0–60, as shown in Fig. 6, which could be attributed to their difference in

DC values. Briefly, a lower DC leads to the release of unbound residual monomers into the culture medium, resulting in the lower cell viability [38,39]. Among these four types of RBCs, the maximum DC was achieved by Esthet-X (76.2 ± 2.6%), followed by RBC 50–20 (71.6 ± 1.1%), Z350 XT (68.3 ± 1.0%), and RBC 0–60 (49.8 ± 0.8%), which was completely in agreement with the cell viability discussed above. Therefore, based on these results, the prescribed RBC 50–20 showed acceptable cytotoxicity.

(2) Cell morphology

The cytotoxicity of RBCs was further confirmed by observing their morphology with FE–SEM, as seen in Fig. 7. After 1 day, larger cell amount could be detected on most RBCs, except that of RBC 0–60 (Fig. 7a), which might be attributed to its lowest DC, as discussed above [38,39]. After 3 and 5 days of culturing, HDPCs cultured onto RBC 50–20 (Fig. 7e, f) and Esthet-X (Fig. 7h, i) showed a more stretched-out morphology, due to their higher DC, compared with those cultured onto RBC 0–60 (Fig. 7b, c) and Z350 XT (Fig. 7k, l). Not only did more cells were found spread out on RBC 50–20 and Esthet-X, but also they interacted with the surface of these two RBCs well by many pseudopodia, which could be detected from their inserted images. Moreover, the interactions also emerged between the HDPCs on RBCs, resulting in the overlap of multilayer cells [40], especially for RBC 50–20 after 5 days of culturing, as shown in Fig. 7(f). These cell morphology observation results corroborated with the above MTT results, confirming the acceptable cytotoxicity of RBC 50–20 and its potential applications for dental restorative materials, compared with Esthet-X.

One of the limitations of this study is that SiO_2 NCs were fabricated using SiO_2 NPs as the only building blocks. Compared with Esthet-X and Z350 XT, although some properties of experimental RBCs, such as DC and polymerization shrinkage could be improved by regulating the filler compositions, their mechanical performance should still be improved greatly, especially considering the application in posterior restorations under higher masticatory force. Based on the discussion above, the increased filler loading and filler packing density of the optimum RBC 50–20 could be further achieved by employing smaller particles directly or using as the building units, which will be carried out in latter our studies.

5. Conclusion

RBCs reinforced with bimodal silica nanostructures presented the improved DC, polymerization shrinkage and mechanical performance, compared with those of RBC 0–60 and RBC 0–70 reinforced with unimodal SiO_2 NCs or SiO_2 NPs, with the introduction of SiO_2 NPs. The obtained RBC 50–20 (SiO_2 NPs:SiO_2 NCs = 50:20, wt/wt) possessed the effectively enhanced physical–mechanical properties and desirable cytotoxicity in vitro, which were comparable with those of Esthet-X, but still requiring modifications. These results suggested that the introduction of bimodal silica nanostructures as fillers with the optimum weight ratio could provide a new gateway to design and synthesize dental RBCs with the enhanced performance. In addition, given to the superior performance of Z350 XT, it could be assumed that the introduction of smaller nanoparticles could have a positive effect on improving the comprehensive properties of RBC 50–20, which will be performed in our future work.

Acknowledgment

This work is financially supported by the High-Tech Research and Development Program of China (2012AA030309), Program for Changjiang Scholars and Innovative Research Team in University (T2011079, IRT1221), National Natural Science Foundation for Distinguished Young Scholar of China (50925312), Project of Shanghai International Science and Technology Cooperation Fund (14520710200), as well as Chinese Universities Scientific Fund (CUSF-DH-D-2013015) for joint financial support.

References

[1] M.M. Karabela, I.D. Sideridou, Dent. Mater. 27 (2011) 825–835.
[2] B. Picka, M. Pelka, R. Belli, R.R. Braga, U. Lohbauer, Dent. Mater. 27 (2011) 664–669.
[3] U. Lohbauer, T. vonder Horst, R. Frankenberger, N. Kramer, A. Petschelt, Dent. Mater. 19 (2003) 435–440.
[4] S. Beun, T. Glorieux, J. Devaux, J. Vreven, G. Leloup, Dent. Mater. 23 (2007) 51–59.
[5] H.H.K. Xu, J.B. Quinn, D.T. Smith, J.M. Antonucci, G.E. Schumacher, F.C. Eichmiller, Biomaterials 23 (2002) 735–742.
[6] J.D. Satterthwaitea, K. Vogel, D.C. Watts, Dent. Mater. 25 (2009) 1612–1615.
[7] J.D. Satterthwaite, A. Maisuria, K. Vogel, D.C. Watts, Dent. Mater. 28 (2012) 609–614.
[8] H. Wang, M.F. Zhu, Y.G. Li, Q.H. Zhang, H.Z. Wang, Mater. Sci. Eng. C 31 (2011) 600–605.
[9] J.L. Ferracane, Dent. Mater. 27 (2011) 29–38.
[10] S.B. Mitra, D. Wu, B.N. Holmes, J. Am. Dent. Assoc. 134 (2003) 1382–1390.
[11] A.R. Curtis, W.M. Palin, G.J.P. Fleming, A.C.C. Shortall, P.M. Marquis, Dent. Mater. 25 (2009) 188–197.
[12] A.R. Curtis, W.M. Palin, G.J.P. Fleming, A.C.C. Shortall, P.M. Marquis, Dent. Mater. 25 (2009) 180–187.
[13] R.L. Wang, S. Bao, F.W. Liu, X.Z. Jiang, Q.H. Zhang, B. Sun, M.F. Zhu, Mater. Sci. Eng. C 33 (2013) 4759–4766.
[14] J.F. Ferracane, E.H. Greener, J. Dent. Res. 63 (1984) 1093–1095.
[15] I.D. Sideridou, M.M. Karabela, E.C. Vouvoudi, Dent. Mater. 27 (2011) 598–607.
[16] S. Rüttermann, I. Dluzhevskaya, C. Großsteinbeck, W.H.M. Raab, R. Janda, Dent. Mater. 26 (2010) 353–359.
[17] X.L. Miao, Y.G. Li, Q.H. Zhang, M.F. Zhu, H.Z. Wang, Mater. Sci. Eng. C 32 (2012) 2115–2121.
[18] R. Du, T.T. Wu, W.J. Liu, L.F. Li, L. Jiang, W.W. Peng, J. Chang, Y.Q. Zhu, J. Endod. 39 (2013) 1023–1029.
[19] J.W. Dai, J. Wang, J.T. Lu, D.H. Zou, H. Sun, Y.F. Dong, Y.B. Yu, L. Zhang, T. Yang, X.L. Zhang, X.D. Wang, G.F. Shen, Biomaterials 33 (2012) 7699–7711.
[20] K. Masouras, N. Silikas, D.C. Watts, Dent. Mater. 24 (2008) 932–939.
[21] K. Baroudi, A.M. Saleh, N. Silikas, D.C. Watts, J. Dent. 35 (2007) 651–655.
[22] G.J. Pearson, Dent. Updat. 17 (1990) 103–108.
[23] S. Kim, J. Jang, Polym. Test. 15 (1996) 559–571.
[24] I.E. Ruyter, H. Øysæd, Acta Odontol. Scand. 40 (1982) 179–192.
[25] F. Goncalves, Y. Kawano, R.R. Braga, Dent. Mater. 26 (2010) 704–709.
[26] M. Atai, D.C. Watts, Z. Atai, Biomaterials 26 (2005) 5015–5120.
[27] A. Peutzfeldt, Eur. J. Oral Sci. 105 (1997) 97–116.
[28] R. Labella, P. Lambrechts, B.V. Meerbeek, G. Vanherle, Dent. Mater. 15 (1999) 128–137.
[29] L.C. Boaro, F. Goncalves, T.C. Guimarães, J.L. Ferracane, C.S. Pfeifer, R.R. Braga, Dent. Mater. 29 (2013) 398–404.
[30] A.A. Razak, A. Harrison, J. Prosthet. Dent. 77 (1997) 353–358.
[31] N. Silikas, G. Eliades, D.C. Watts, Dent. Mater. 16 (2000) 292–296.
[32] P.R. Braga, J.L. Ferracane, J. Dent. Res. 81 (2002) 114–118.
[33] H.Q. Zhang, B.W. Darvell, Dent. Mater. 28 (2012) 824–830.
[34] H. Lu, Y.K. Lee, M. Oguri, J.M. Powers, Oper. Dent. 31 (2006) 734–740.
[35] S.A.R. Junior, C.H. Zanchi, R.V. de Carvalho, F.F. Demarco, Braz. Oral Res. 21 (2007) 16–21.
[36] P. Padipatvuthikul, F.D. Jarad, L. Mair, Wear 268 (2010) 1483–1489.
[37] J.W. Kim, L.U. Kim, C.K. Kim, Biomacromolecules 8 (2007) 215–222.
[38] S. Krifka, G. Spagnuolo, G. Schmalz, H. Schweikl, Biomaterials 34 (2013) 4555–4563.
[39] N. Jagdish, S. Padmanabhan, A.B. Chitharanjan, J. Revathi, G. Palani, M. Sambasivam, K. Sheriff, K. Saravanamurali, Angle Orthod. 79 (2009) 1133–1138.
[40] Z.G. Chen, H.Y. Liu, X. Liu, X.J. Lian, Z.W. Guo, H.J. Jiang, F.Z. Cui, Mater. Sci. Eng. C 33 (2013) 1048–1053.